Faraday Discussions

Accepted Manuscript

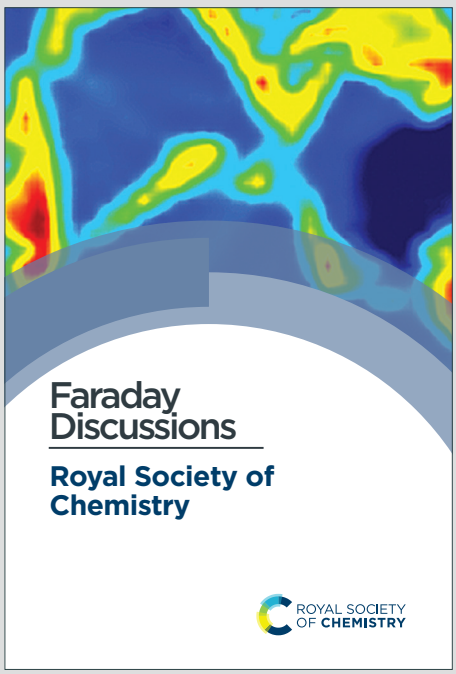

This article can be cited before page numbers have been issued, to do this please use: Z. Xia, V. Bellani, J. Sun and V. Palermo, *Faraday Discuss.*, 2020, DOI: 10.1039/C9FD00123A.

ROYAL SOCIETY OF CHEMISTRY

www.rsc.org/faraday_d

View Article Online
DOI: 10.1039/C9FD00123A

Electrochemical exfoliation of graphite in H_2SO_4, Li_2SO_4 and $NaClO_4$ solutions monitored in-situ by Raman microscopy and spectroscopy

Zhenyuan Xia[1,2*], Vittorio Bellani[3], Jinhua Sun,[1] Vincenzo Palermo[1,2]

[1]Industrial and Materials Science, Chalmers University of Technology, Hörsalsvägen 7A, 41258 Göteborg, Sweden

[2]Istituto per la Sintesi Organica e la Fotoreattività, CNR, via Gobetti 101, 40129 Bologna, Italy

[3]Dipartimento di Fisica, Università degli Studi di Pavia and INFN, via Bassi 6, 27100 Pavia, Italy

Abstract

The electrochemical exfoliation of graphite is one of the cheapest and most tunable industrial techniques to produce graphene nanosheets with tunable degree of oxidation and solubility. Anodic oxidation allows high-yield production of electrochemically exfoliated graphene oxide (EGO) in either acids or salt solutions, with the key role played by ions electrochemically driven in between the graphene sheets. This chemical intercalation is followed by a mesoscale mechanical exfoliation process, which is key for the high yield of the process, but which is still poorly understood. In this work, we use Raman spectroscopy to simultaneously monitor the intercalation and oxidation processes taking place on the surface of highly ordered pyrolytic graphite (HOPG) during electrochemical exfoliation. The mechanism of EGO formation in either acidic (0.5 M H_2SO_4) or neutral (0.5 M Li_2SO_4) electrolytes through blistering and cracking steps is discussed and described. This process is compared also to non-destructive intercalation of graphite in an organic electrolyte (1 M $NaClO_4$ in acetonitrile). The results obtained show how high exfoliation yield and low defectivity shall be achieved by the combination of efficient, non-destructive intercalation followed by chemical decomposition of the intercalants and gas production.

View Article Online
DOI: 10.1039/C9FD00123A

Introduction

The electrochemical exfoliation of graphite is one of the cheapest and most versatile ways to produce 2-dimensional soluble nanosheets. The exfoliation can be easily tuned varying applied potential and electrolyte, to obtain a wide range of 2D materials, from pristine graphene to highly processable graphene oxide. The electrochemical process is well-known and used industrially for the synthesis of graphite intercalated compounds (GICs) with reversible intercalation/deintercalation properties.[1] One of the most relevant applications of GICs is as lithium (Li) anodes for rechargeable Li-ion batteries.[2, 3] After the discovery of graphene, the electrochemical exfoliation process has also been extensively studied for the production of graphene sheets.[4, 5] Typically, the electrochemical exfoliation can be seen as an 'over-oxidation' process of the GIC compounds, which involves the formation of GICs with unstable electrolytes at high electric field, and the subsequent destructive delamination of GICs layers.[6] The use of electrochemistry allows to have a step-controllable oxidation process of graphite by varying the polarity of bias applied,[7, 8] the use of aqueous or non-aqueous solutions,[9, 10] or the concentration of the active electrolytes.[11, 12] The tunability of electrochemistry permits a better control of the oxidative damage of the sheets, an eco-friendly process with less consumption of harsh acid, and a faster production rate as compared to the traditional chemical exfoliation (e.g. Hummer's method) approach.[13] The high tunability, environmental sustainability and low cost of this technique are already used for large-scale production of graphene-based materials.[14]

Anodic exfoliation allows high-yield production of electrochemically exfoliated graphene oxide (EGO) sheets with different degree of oxidation. The most widely used electrochemical production technique is the anodic exfoliation of graphite in either dilute mineral acid or salt electrolytes. For example, Su et al. developed electrochemical exfoliation of EGO in 0.5 M H_2SO_4 using high bias, + 10 V.[15] Parvez et al. reported anodic exfoliation of graphite with 0.1 M $(NH_4)_2SO_4$ aqueous electrolyte to obtain low defect EGO flakes, with a high yield (>80%) of one- to three-layer graphene flakes, high C/O ratio (12.3) and low sheet resistance (4.8 kΩ/sq for a single EG sheet).[16] We previously reported EGO production with >50% mono and bilayers, C/O ratio (12.7) and >1 μm flake size, able to be processed in electrodes with 20 Ω/sq sheet resistance.[17]

View Article Online
DOI: 10.1039/C9FD00123A

We also described an two-step exfoliation approach based on intercalation of uncharged acetonitrile molecules with charged perchlorate, followed by decomposition due to microwave irradiation.[17] More recently, Pei et al. and Cao et al. independently reported a two-step approach to achieve full exfoliation of EGO with high oxygen contents, where H_2SO_4-GICs were formed by electrochemical intercalation and then exfoliated in dilute H_2SO_4 or $(NH_4)_2SO_4$ electrolyte.[18, 19]

Despite significant efforts to improve EGO production and study its chemistry, the mechanism of its formation on the bulk graphite during anodic process has been rarely reported. It is not clear which electrolyte, solvent and experimental conditions have the best potential to achieve high yield and good quality. Few studies performed systematic comparisons, mainly based on structural analysis of morphology of the exfoliated surface acquired by SEM or AFM.[13, 20] In the present work, we improve this approach combining optical microscopy and Raman spectroscopy to map, in real time, the chemical disruption of the graphite surface during electrochemical exfoliation in different conditions.

Raman spectroscopy is a powerful non-destructive method for quantitative analysis of carbon-based materials.[21] In particular, *in-situ* Raman mapping of bulk graphite flakes allows us to identify directly the intercalation efficiency, defect concentration, and lattice disruption of graphite during the anodic oxidation process.[22] We acquired Raman data with high spatial (~ 3 μm) and spectral resolution (0.8 cm^{-1}) during exfoliation of graphite in two types of aqueous electrolytes (0.5 M H_2SO_4, 0.5 M Li_2SO_4). This allowed to reveal the intermediate reaction products during the 'over-oxidation' and surface deformation process. The Raman data allowed to compare the EGO formation mechanism in acid and neutral sulfate ion based aqueous solutions. The observed chemical changes were also compared with a similar anodic process under a non-aqueous electrolyte (1 M $NaClO_4$ in acetonitrile), which instead features a non-oxidative intercalation reaction.

Experimental

HOPG (12 mm × 12 mm × 2 mm, Grade ZYH) was purchased from GE Advanced Ceramics and exfoliated into thin pieces of size 12 mm × 12 mm × 0.05 mm by scotch tape. Sulfuric acid (Sigma-Aldrich, 95–97%), lithium sulfate (Sigma-Aldrich, 99%) were used as the electrolytes for the electrochemical oxidation of HOPG surface in aqueous solution.

View Article Online
DOI: 10.1039/C9FD00123A

Sodium perchlorate (Sigma-Aldrich, 98%) was used as the electrolyte for anodic intercalation of HOPG in acetonitrile (Sigma-Aldrich, anhydrous, 99.8%) solution.

The electrochemical exfoliation cell included a piece of HOPG, used as working electrode, and copper foil, used as counter electrode. Figure 1 shows the setup of our electrochemical platform. The HOPG electrode (1.2 x 1.2 cm) was obtained by scotch tape exfoliation and had an average thickness of around 0.05 mm, and attached to a Cu foil through silver glue. The side faces of working electrode were sealed with the epoxy glue to prevent exposure of the HOPG edges to the electrolyte. Both working and counter electrodes were fixed by a double side scotch tape on a glass substrate. The electrolyte solution was added on the graphite and Cu foil surface and covered with a glass slide.

The electrolytes used in this work were 0.5 M H_2SO_4 (pH≈0.3) or 0.5 M Li_2SO_4 (pH≈7) in water and 1 M $NaClO_4$ in acetonitrile. The anodic exfoliation of graphite was carried out under a potential of +3 V in acidic and mineral salt electrolytes and + 5 V in organic electrolyte respectively, at room temperature. In all cases, we used two electrodes system, and the setup value (+3 V or +5 V) is the total voltage. Raman scattering measurements were carried out with a micro-Raman spectrometer (Model: LabRAM from Horiba Jobin-Yvon), using a 50 × objective (laser spot diameter ≈ 2 μm), laser excitation wavelength of 632.8 nm and laser power < 1 mW to avoid heating of the sample. The Raman mapping mode was used over a scan area of around 63 x 63 μm. For each oxidation time step we collected ca. 800 spectra to study in particular the two band regions at 1070 cm^{-1} – 1970 cm^{-1} (G band) and 2330 cm^{-1} to 3050 cm^{-1} (2D band).

Results and Discussion

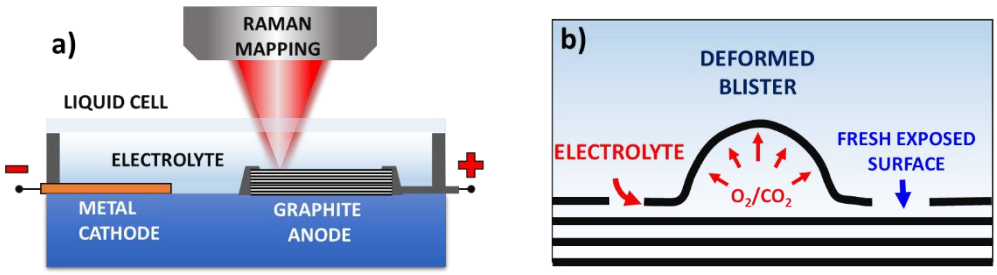

Figure 1. a) Schematic illustration of the Raman setup for in situ spectroscopic monitoring of the graphite exfoliation process, b) schematic of the graphite exfoliation process during electrochemical oxidation.

View Article Online
DOI: 10.1039/C9FD00123A

Figure 2a and S1a-c shows the optical images of the HOPG surface (image size ≈63 x 63 μm) immersed in 0.5 M H_2SO_4 solutions after applying a bias of + 3 V for 5 s, 60 s, 300 s, and 600 s respectively. Blistering was observed after just 5 seconds, which is consistent with previous studies on electrochemical graphite exfoliation.[13, 20] These blisters originated from the intercalation and oxidation of solvated anions and the subsequent evolution of gas (e.g. O_2 from water electrolysis, and CO_2 from carbon oxidation, see also scheme in Figure 1b). The process is so fast and visible on mesoscopic scale because the applied potential is much higher than the thermodynamic potential for carbon and water oxidation (E_{carbon} = +0.95 V and E_{O2}= +1.23 V, respectively). Further oxidation led to the accumulation and migration of gases in the uppermost graphite layers. Trapped gases could build up a high pressure (several thousand bar)[13] inside the blisters, elastically deform the graphene multilayers, and finally erupt from the inner graphite layers with the formation of cellular structure cracks around the giant blisters, as shown in Figure 1b and 2a, S1b. The periodic cracking of the uppermost graphene layers and the infiltration of electrolytes through these cracks to the layers underneath results in continuous oxidation and blister evolution, and the final delamination of EGO multilayers from the surface, with a corresponding roughening visible by optical microscopy (Figure S1c). The scale of blistering and mechanical fragmentation caused by gas expansion limits the size of EGO sheets within tens of micrometer scale during the electrochemical oxidation process, at difference with chemical methods which can yield GO sheets with sizes >100 μm.[23]

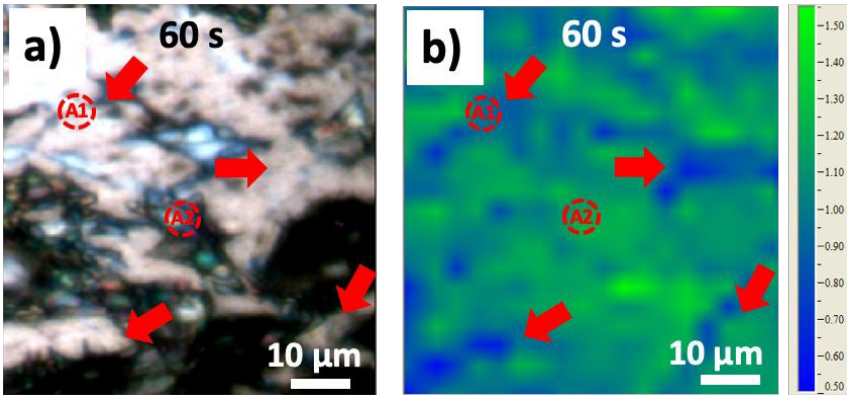

Figure 2. a) Optical image of HOPG surface and b) the corresponding I_D/I_G Raman mapping image after 60 seconds' electrochemical oxidation in 0.5 M H_2SO_4 electrolyte.

View Article Online
DOI: 10.1039/C9FD00123A

It is worth noting that some reports attribute the blistering and fragmentation to SO_2 gas formed during anodic exfoliation of graphite in dilute H_2SO_4 solution.[24] However, the reduction of dilute H_2SO_4 is thermodynamically very difficult, while the anodic conversion of SO_2 to H_2SO_4 is a spontaneous exothermic process.[6, 25] The release of SO_2 only happens under extreme conditions such as "thermal shock" treatment of H_2SO_4-GIC composites, in which graphite was fully intercalated with concentrated H_2SO_4.[26] In case of acid solutions, the gas source comes mainly from CO_2 produced by the corrosion of the carbon anode and from oxygen produced by water electrolysis.[13]

We used Raman spectroscopy to monitor the graphite surface during the anodic process, to explore the structural and chemical changes due to intercalation and oxidation process. A total of 3200 spectra were acquired on each sample to monitor G and 2D bands. The G peak at ~ 1580 cm^{-1} in the Raman spectra is the typical signature of sp^2 hybridized carbon structure; while the D peak at ~ 1330 cm^{-1} is due to inter-valley resonant Raman scattering, indicative of lattice defects, as example caused by oxidation. The ratio of the intensity of D peak and G peak (I_D/I_G) allowed to estimate the average defect density on the graphite surface. Figure 2b and S1d-f show the I_D/I_G maps acquired simultaneously to optical images in Figure 2a and S1a-c, on the same areas of the sample. During the first 5 s oxidation, an average I_D/I_G value of 0.14±0.13 was observed, mainly due to small blisters and step edge sites. Further anodic oxidation (Figure 2b, S1b) led to a dramatic increase of the I_D/I_G ratio, due to the SO_4^{2-} intercalation and the subsequent oxidation of graphite in correspondence of grain boundaries or step-edges. I_D/I_G increased to 1.06±0.16 after 60 s and 1.89±0.21 after 300 s. Interestingly, the "valley" areas nearby giant blisters showed I_D/I_G value lower than the average (deep blue in the color scale in Figure 2b and S1d-f, with red arrows indicating the "valley" region). As example, the average I_D/I_G in the "valley" area was 0.81±0.12 after 60 s and 1.55±0.13 after 300 s, indicating that the cracks due to blistering were exposing fresh, less defective layers of the underlying bulk graphite (as exemplified in scheme in Figure 1b). For longer oxidation times (600 s), the I_D/I_G map became more uniform, with an average I_D/I_G value of 1.51±0.08, similar between the crack and blisters, indicating a steady state due to continuous delamination of uppermost EGO layers and the continuous oxidation of inner layers.

View Article Online
DOI: 10.1039/C9FD00123A

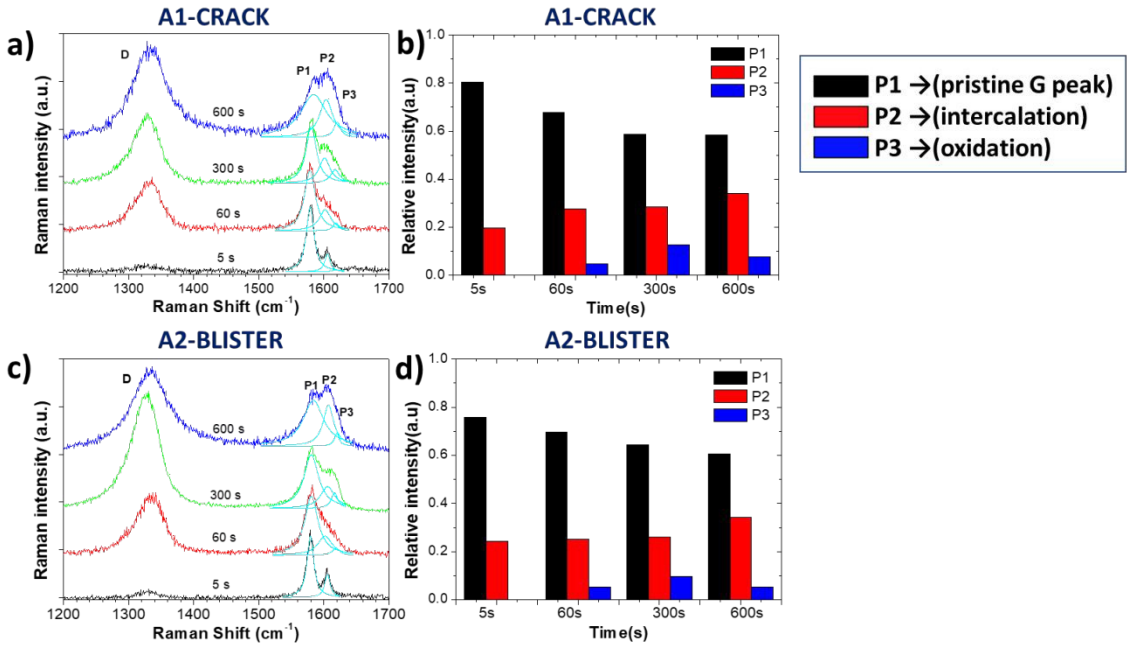

Figure 3. Raman spectra acquired from certain areas of HOPG surface during electrochemical oxidation in 0.5 M H_2SO_4 electrolyte, a,c) Raman spectra in D, G band region for A1 and A2 area, b,d) Evolution with increasing time of Raman P1, P2 and P3 peaks for A1 and A2 area.

Figure 3 and Table 1 show more detailed Raman spectra taken from two representative areas, A1 and A2, localized on a "valley" area corresponding to surface crack and on a blister respectively. In both areas the increase of D peak is similar to what we already observed for the I_D/I_G ratio mapping images. There was a broadening trend of D peak and G peak on both selected areas, indicating a crystalline damage and amorphization of graphite layers due to oxidation (see in Table 1). As example, the Full width at half maximum (FWHM) value of D peak (named as Γ_D) in A1 area increased from 46±6 cm^{-1} (5 s) to 64±6 cm^{-1}(600 s), and the FWHM value of G peak (named as Γ_G) increased from 14±2 cm^{-1}(5 s) to 47±6 cm^{-1}(600 s) on A1 and A2 area respectively. During oxidation from 60 s to 300 s, the D peak increased more on the giant blister A2 area (I_D/I_G =2.01) compared to the valley A1 area (I_D/I_G =1.46).

View Article Online
DOI: 10.1039/C9FD00123A

Table 1. Variation of the Raman spectra parameters of graphite during anodic oxidation in 0.5 M H_2SO_4

Time (s)	ω_D (cm^{-1})	Γ_D (cm^{-1})	ω_G (cm^{-1})	Γ_G (cm^{-1})	I_D/I_G	L_a(nm)	n
A1 (0.5 M H_2SO_4)							
5 s	1327	46.1	1579	13.8	0.24	186.9	10.1
60 s	1330	50.2	1578	19.4	1.02	37.3	6.9
300 s	1326	52.0	1580	20.0	1.46	25.9	6.1
600 s	1333	64.3	1585	46.8	1.45	26.1	5.4
A2 (0.5 M H_2SO_4)							
5 s	1329	41.0	1579	12.4	0.09	425.4	8.2
60 s	1333	52.9	1583	27.6	1.20	31.6	7.5
300 s	1325	52.6	1582	31.9	2.01	18.9	7.0
600 s	1334	68.0	1584	41.1	1.51	25.1	5.6

Also the G band changed significantly after the 5 s oxidation process, becoming the convolution of three different peaks named P1, P2 and P3[13] for clarity, according to their position from low to high wavenumbers:

-P1=1577 cm^{-1} corresponds to the standard G peak due to the $E_{2g2}(i)$ mode stretching of the carbon atoms, and indicates the presence of bulk graphite.

-P2=1605 cm^{-1} is instead the $E_{2g2}(b)$ mode of carbon atoms adjacent to intercalants, and indicates the presence of intercalated graphite.

-P3=1617 cm^{-1} (also termed D' band) appears upon further oxidation due to large scale damage and deformation, indicative of surface oxidation.

Figure 3b,d shows the evolution of P1, P2 and P3 on the selected A1 and A2 areas. Both areas show a similar trend in the increase of P2 peak, indicating a continuous intercalation of $HSO4^-$ into the graphite basal plane with the formation of $C^+HSO_4^-$ GIC composite. P3 peak increased initially, but decreased upon long exfoliation times. The reduction in defectivity can be explained only by the continuous mechanical removal of the upper, highly oxidised layers, exposing the pristine surface underneath.

The intensity ratio of the P1 and P2 peaks is related to the intercalation stage index n by means of

$$P1/P2 = \sigma_i/\sigma_b * (n-2)/2 \quad (1)$$

where σ_i/σ_b (assumed equal to 1) is the ratio of the cross-section of Raman scattering from interior and bounding layers.[27] In both A1 and A2 area, the intercalation stage index

View Article Online
DOI: 10.1039/C9FD00123A

estimated from the evolution of G-peak splitting (Table 1) continuously decreased from $n \approx 10$ (5 s) to $n \approx 7$ (60 s) and $n \approx 5$ (600 s). The observation is consistent with the previous reports, and it also explains the difficulty for obtaining single layer EGO due to the insufficient intercalation of HSO_4^- anions in acid.[28]

We also used the I_D/I_G ratio to evaluate the changes in graphite crystalline structure using the formula:[29, 30]

$$L_a = \frac{560}{E_{laser}^4}\left(\frac{I_D}{I_G}\right)^{-1} \quad (2)$$

Where L_a is the crystalline size of graphite, E_{laser} is the laser excitation energy (1.96 eV), I_D/I_G ratio is obtained experimentally. The calculated L_a are summarized in Table 1, together with the values of the Raman D and G peak position, width and I_D/I_G ratio. The average graphite crystalline size L_a decreased from hundreds nm to ~26 nm due to the amorphization and disorder introduced by oxidative destruction of graphite.

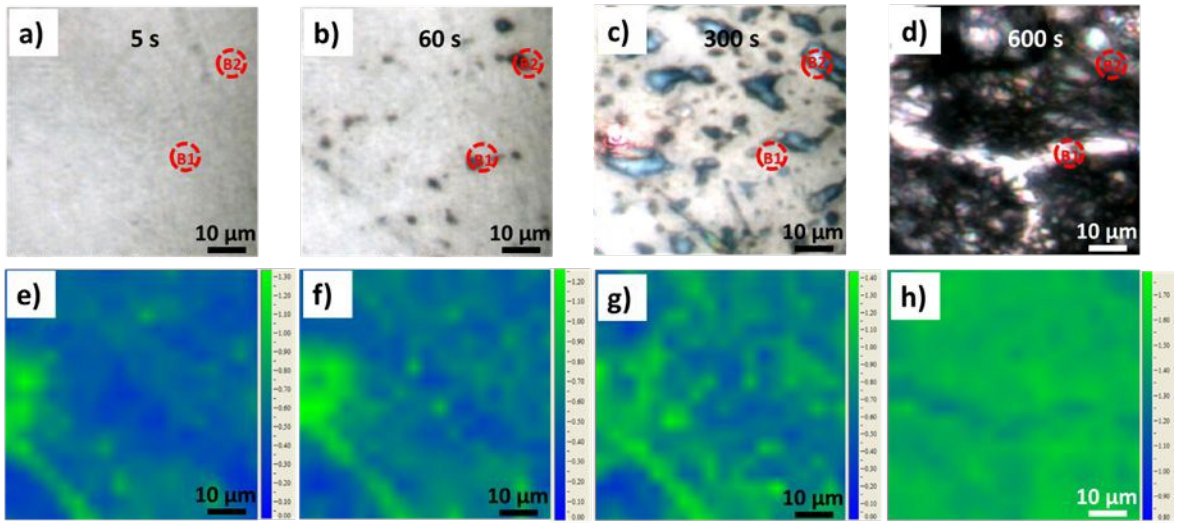

Figure 4. a-d) Optical images of HOPG surface during electrochemical oxidation in 0.5 M Li_2SO_4 electrolyte and e-h) the corresponding I_D/I_G Raman mapping images.

Besides D and G bands, we also monitored the 2D band (Figure S2) on A1 and A2 areas. The 2D band (often named G') originates from a two-phonon resonance Raman processes, and it is the second prominent band on graphite in addition to the G band. We could observe a sharp 2D peak at ~ 2685 cm^{-1} after 5 s oxidation, similar to the pristine graphite 2D peak. The 2D peak became broader and its relative intensity was lower with the longer oxidation

View Article Online
DOI: 10.1039/C9FD00123A

time. 2D band is usually used to determine graphene layer numbers; however, electrochemical oxidation broke the stacking order of adjacent graphene layers and introduced amorphization of carbon atoms. Therefore, the 2D peak was too weak to estimate the layer number information of delaminated EGO sheets.

Meanwhile, new peaks with low intensity appeared at 2880 – 2950 cm^{-1} in both A1 and A2 area, due to the D+D' bands, indicative of high defect density.

Besides graphite exfoliation in mild acid, we also studied exfoliation in neutral salts. Figure 4a-d shows the optical images of the graphite surface upon exfoliation at +3 V in 0.5 M Li_2SO_4 solutions, recorded at 5 s, 60 s, 300 s, and 600 s. Blistering was observed, even if less rapid than what observed in acids at similar oxidation times. The process was slower, and we could also see the migration of giant blisters and fragmentation of the superficial EGO layers with the size dimension of around 30-60 μm. Meanwhile, *in situ* Raman mapping was performed on the graphite basal surface as well (Figure 4e-h). The I_D/I_G showed much smaller increase during the oxidation going from 0.62±0.19 at 5 s to 0.66±0.20 after 60 s to 0.90±0.24 after 300 s. Though, we observed a clear distribution of the oxidation related defects nearby the step edges and blisters' area, see Figure 4e-g. After 600 s oxidation (Figure 4h) the average I_D/I_G reached 1.48±0.07, with the distribution of lower defective areas (I_D/I_G value ~ 1.2) along the crack region of graphite basal plane.

In order to have a detailed analysis of the Raman spectra variation, we compared also in this case two representative areas, B1 and B2, on the crack and blister sites of the graphite surface respectively (Figure 5a,c). The D peak increased during the oxidation; however, we observed no clear D peak broadening in both B1 and B2 region (see in Table 2), only a broadening of the G peak. Γ_G value increases from 14 (5 s) to 29 (600 s) on B1 area and from 15 (5 s) to 38 (600 s) on B2 area. The I_D/I_G value on the B2 blister area increased to 0.98 after 300 s oxidation period, significantly higher than what observed on the B1 crack area (I_D/I_G=0.71). This is consistent with what observed in acid, with a more destructive intercalation/oxidation process below the blisters' region, as compared to the "valley" area before cracking. After 600 s, the I_D/I_G ratio reached a value on B2 and B1 areas of 1.68 and 1.59 respectively, indicating the full oxidation of the uppermost layers and continual intercalation/oxidation of the innermost layers.

View Article Online
DOI: 10.1039/C9FD00123A

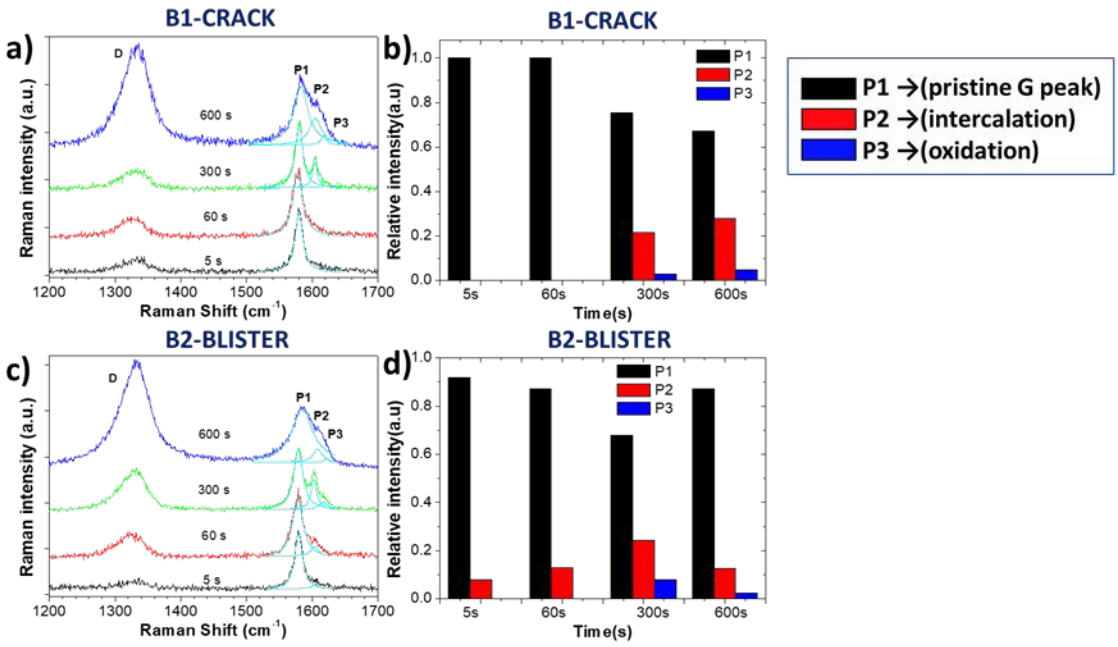

Figure 5. Raman spectra acquired from certain areas of HOPG surface during electrochemical oxidation in 0.5 M Li_2SO_4 electrolyte, a,c) Raman spectra in D, G band region for B1 and B2 area, b,d) Evolution with increasing time of Raman P1, P2 and P3 peaks for B1 and B2 area.

While the evolution of the D peak was qualitatively similar to what observed in acid, the evolution of P1, P2 and P3 peaks was significantly different. Unlike the rapid intercalation process in acid electrolytes, sulfate anion intercalation in neutral salt solutions is a much slower process. Our observation is consistent with the report of Alsmeyer et al. for mild acid condition, since weaker acid strength lead to a higher intercalation potential for the formation of GICs.[31] P1 peak on the crack are did not vary much during the first 60 s, indicating the presence of pristine graphite. On the B2 blister, a low intensity P2 peak from G band was observed (Figure 5a,c), attributed to the intercalation of SO_4^{2-} on step edges and defects region of graphite. For longer times (t>300 s), the presence of P2 and P3 peaks was observed instead in all areas, similar to the exfoliation in acid (Figure 5b,d).

View Article Online
DOI: 10.1039/C9FD00123A

Table 2. Variation of the Raman spectra parameters of graphite during anodic oxidation in 0.5 M Li_2SO_4

Time (s)	ω_D (cm^{-1})	Γ_D (cm^{-1})	ω_G (cm^{-1})	Γ_G (cm^{-1})	I_D/I_G	L_a(nm)	*n*
B1 (0.5 M LI_2SO_4)							
5 s	1331	46.7	1580	14.0	0.61	61.6	-
60 s	1325	46.9	1578	19.4	0.67	56.4	-
300 s	1328	53.2	1580	13.7	0.71	53.2	9.0
600 s	1332	51.0	1584	29.2	1.59	23.9	6.8
B2 (0.5 M Li_2SO_4)							
5 s	1329	48.9	1579	14.8	0.59	64.3	24.9
60 s	1322	55.8	1578	19.7	0.68	56.1	15.6
300 s	1327	50.6	1578	16.3	0.97	38.6	7.6
600 s	1331	53.5	1585	37.8	1.68	22.6	17.1

The intercalation stage index *n* decreased from $n \approx 25$ to $n \approx 8$ on B2 area and $n \approx 7$ (600 s) on B1 area, indicating a successful intercalation of SO_4^{2-} ion on graphite layers.

However, *n* on B2 blister area increased again, reaching $n \approx 17$ after 600 s oxidation. This cannot be explained with a chemical de-intercalation of sulfate ions, but was instead attributed to the delamination and removal of the uppermost EGO layers, exposing partially fresh graphite underneath.

As observed for the exfoliation in acid, also here the average graphite crystalline size L_a decreased going from around hundred nm to ~23 nm and the 2D band broadened (Figure S3).

We should underline that, in our setup, Raman spectra were acquired on microscopic scale, with high spatial resolution, at difference with typical Raman spectra which just report an average signal from a macroscopic area of the sample. The 3200 Raman spectra we acquired on different samples at different exfoliation stages allowed us to perform a statistical analysis of the data, correlating the different processes ongoing in each point of the sample.

Figure 6a correlates the intensity of P2 peak (indicative of ions intercalation) and of P3 peak (indicative of sample oxidation) for the sample treated in sulfuric acid. Correlation is poor at initial stages (t= 5 and 60 s). For later stages, a clear linear correlation is observed, indicating that graphene oxidation is more intense in areas where intercalation is strong. The highest correlation is observed for t=300 s; then, in agreement with what observed in

View Article Online
DOI: 10.1039/C9FD00123A

specific points in the sections above, the average value of P3 decreases, but the correlation between the two processes is still evident.

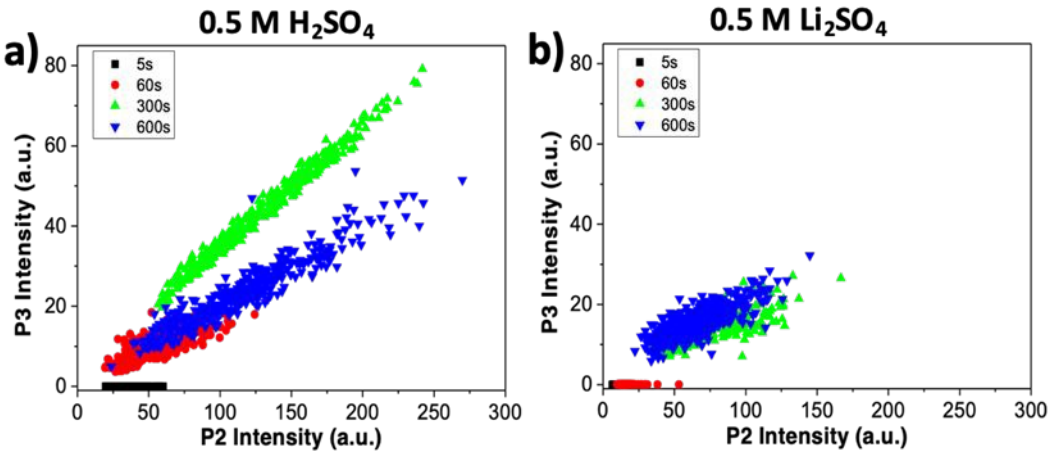

Figure 6. Correlation between intercalation (P2) and oxidation of the sample (P3), obtained from Raman maps at different oxidation times. Graphs refer to a) treatment in sulfuric acid and b) treatment in lithium sulfate.

Figure 6b performs the same analysis for samples treated in lithium sulfate. P3 intensity is zero at t=0 s and 60 s. Oxidation becomes significant only in later stages, but even then, no clear correlation is observed indicating that the oxidation in neutral media is much lower than in acid, and is not directly correlated to intercalation.

Combined use of P1, P2 and P3 data allowed to obtain even more refined insight, as shown in Figure 7. Here, the intercalation stage calculated using formula (1) is correlated with the graphene oxidation for each point of all the samples. We shall observe that strongly oxidized areas (on the right part of the graph) show on average lower intercalation numbers than poorly oxidized areas, again confirming that the oxidation process is directly correlated to the ions' intercalation. Noteworthy, the value of *n* seems to reach an asymptotic value for a given treatment time, not directly correlated to the oxidation values. Also in this case, oxidation values decrease from t=300 s to t=600 s, due to the first areas to be removed from the sample being the ones most oxidized. The average intercalation stage, however, decreases slightly, indicating that, while oxidized areas exfoliated by the blisters are removed, highly intercalation continues in the uncovered areas of the samples.

View Article Online
DOI: 10.1039/C9FD00123A

Conversely, samples treated in lithium sulfate showed no P3 peak for t<60 s, and only random correlation for t >60 s (not shown).

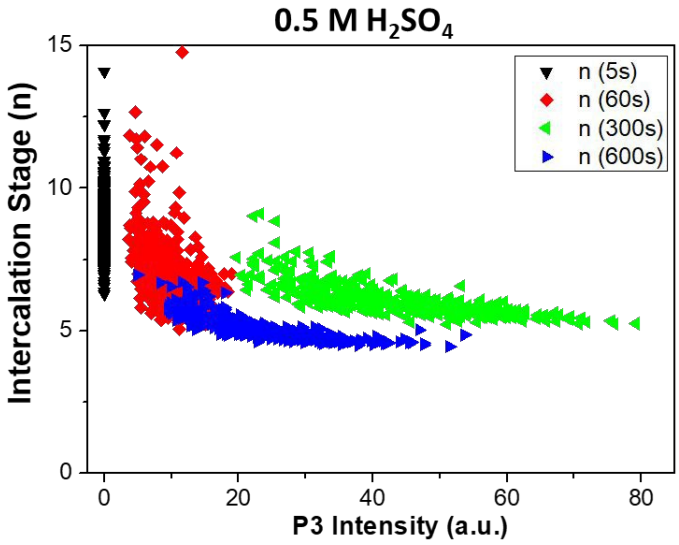

Figure 7. Correlation between the intercalation stage of ions in graphite (P1/P2 calculated with formula 1 in main text) and oxidation of the sample (P3), obtained from Raman maps at different times. Graphs refer to treatment in sulfuric acid. Samples treated in lithium sulfate showed no P3 peak for t<60 s, and only uncorrelated data for t>60 s.

The systematic optical and Raman comparison of the anodic process in acid or neutral salt solution indicates the most plausible model of EGO formation: first, solvated sulfate ions (HSO_4^-/SO_4^{2-} in acidic media and SO_4^{2-} in neutral media) intercalate into the graphite grains or step-edges under a critical potential > 1.8 V (vs RHE) with the formation of GICs.[13, 31] Intercalation proceeds till reaching an intercalation stage $n \geq 5$.

Second, electrolysis of the co-intercalated water molecules releases large amount of O_2 gas, Water induced hydrolysis of the GICs complex leads to oxidative cleavage of carbon atoms from the edges or defects of the graphite accompanied by CO_2 gas due to decomposition of GICs. Third, the almost simultaneous gas evolution and oxidation process driven by chemical and physical forces results in a rapid blister growth. The deformed blisters crack the upper graphene layers, uncovering pristine graphite areas in the cracks between the blisters (Figure 1b). The collapse of the giant blisters mechanically peels off the uppermost EGO flakes, and cycle can start again. The penetration of solvated

View Article Online
DOI: 10.1039/C9FD00123A

anions on the crack edges brings repeatable intercalation, gas formation and graphite oxidation process from the inner layers.

We should underline that our *in-situ* monitoring process only focused on the basal face of graphite, in order to have a clear visualization of the surface morphology changes. However, in practical exfoliation, the side faces will also be included during the whole intercalation, oxidation and expansion steps, giving an even faster exfoliation process.

It is known that water plays an important role in the EGO production. The water molecule is not only the source of oxygen gas caused by water electrolysis, but also the attacking nucleophile during the oxidative hydrolysis of GICs complex.

In a previous work, we estimated the average thickness of the produced EGO nanosheets using Atomic force microscopy (AFM) statistical analysis. The nanosheets feature a "sandwich" structure with multilayer configurations instead of single layer.[28] The present work provides a mechanistic understanding of this limit, revealing that the intercalating anions reach at best an intercalation stage $n \geq 5$ in dilute acidic or neutral media. Furthermore, the blister-crack formation-collapse mechanism of the uppermost graphene layers limits the lateral dimension of the exfoliated EGO sheets to tens of micrometer (around 30-60 μm in our experiment).

Although EGO exfoliation in salts looks qualitatively similar to exfoliation in acids, there is still some difference between the two media. 1) Energetically favorable intercalation of sulfate anions in acidic media is evidenced from the faster growth of P2 peak during the initial stages of oxidation (t< 60 s), indicating a more efficient intercalation process and possibly more thermodynamic stable GICs complex in acid instead of neutral solution[13]:

$$\mathrm{C}_p + \mathrm{HSO}_4^- + \gamma\mathrm{H_2O} \leftrightarrow \mathrm{C}_p^+ \cdot \mathrm{HSO}_4^- \cdot \gamma\mathrm{H_2O} + e^- \quad (3)$$

2) meanwhile, carbon corrosion potential in neutral condition is lower than in acid condition, corresponding to the irreversible oxidative reactions[13,32]:

$$\mathrm{C}_p^+ \cdot \mathrm{HSO}_4^- + \mathrm{H_2O} \xrightarrow[-H_2SO_4]{} \mathrm{C}_p^+ \cdot \mathrm{OH}^- (sp^2) \rightarrow C_p \cdot \mathrm{OH}\ (sp^3) \quad (4)$$

and the following electrochemical related carbon dioxide formation[13,32]:

$$C_p \cdot \mathrm{OH} + \mathrm{H_2O} \rightarrow C_{p-1} + \mathrm{CO_2} + 3\mathrm{H}^+ + 3e^- \quad (5)$$

water electrolysis in neutral solution also requires lower oxidation potential as compared to the acid solution[33]:

View Article Online
DOI: 10.1039/C9FD00123A

$$2H_2O \rightarrow O_2 + 4H^+ + 4e^- \quad (6)$$

which means that more oxygen gas will be produced in neutral solution, and more carbon will be oxidized in neutral solution as compared to acids.

Thus, while in acids graphite intercalation and exfoliation are directly correlated to graphite oxidative damage, in salt the two processes are not well correlated, as clearly shown by the statistical analysis in Figures 6 and 7.

Although less blistering was observed initially in Li_2SO_4 respect to H_2SO_4 due to the lower intercalation efficiency, the fast gas evolution from neutral media resulted in a rougher morphology after long time oxidation.

Should though be noted that the action of water will improve the production efficiency of gas source, which might avoid serious damage of EGO sheets during the mechanical expansion step, but the rapid exfoliation process also leading to incomplete intercalation of graphite and formation of more multiple layer EGO. Thus, electrochemical exfoliation in neutral salts (in this case, Li_2SO_4) could give higher yield but thicker graphene than exfoliation performed in diluted sulfuric acid (H_2SO_4).

3) The whole process removes mechanically EGO nanosheets with a thickness of few layers and a lateral size of tens of μm, continuously uncovering fresh areas of graphite to be exfoliated. This gives an experimental explanation for the high production speed attained with electrochemical exfoliation at industrial level.

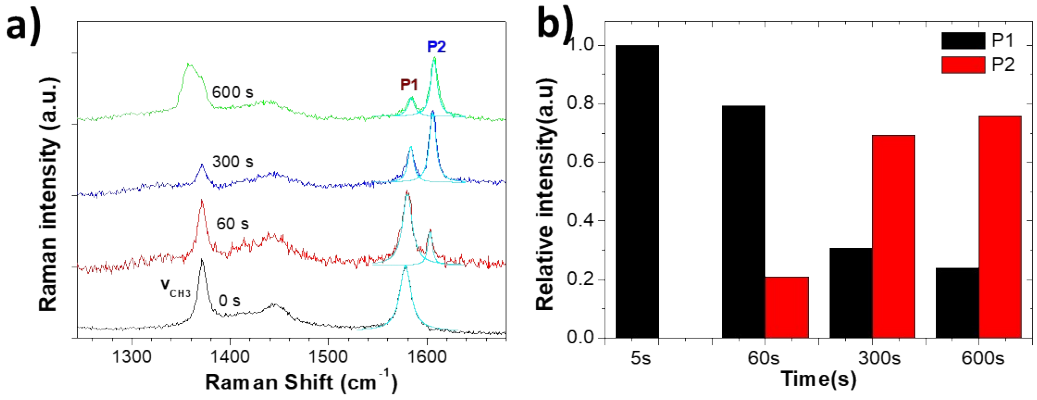

Figure 8. a) Raman spectra acquired from HOPG surface during electrochemical oxidation in 1 M $NaClO_4/CH_3CN$ electrolyte. b) Evolution with increasing time of Raman P1, P2 peaks.

View Article Online
DOI: 10.1039/C9FD00123A

Finally, to further study the role of water in the electrochemical process, we used our setup to monitor the anodic graphite intercalation with a non-aqueous electrolyte. Figure S4a-d shows the optical images of a graphite surface in 1 M $NaClO_4$ in acetonitrile (CH_3CN). To achieve some visible effect, a bias of + 5 V instead of +3 V should be applied for t=0 s, 60 s, 300 s, and 600s.

After 60 s oxidation, few blisters formed on the graphite surface, but there was no major change in surface morphology under prolonged treatment. Raman measurements showed the characteristic G and 2D peaks of graphite (Figure 8a, S5). In the G band region, two peaks of acetonitrile at 1370 cm^{-1} and 1449 cm^{-1} were observed due to the CH_3 deformation vibration. Other peaks at 2248 cm^{-1} and 2942 cm^{-1} were due to the C=N stretching and C-H stretching vibration modes of acetonitrile, respectively (Figure S5).[34]

We could not observe any D peak formation at ~ 1330 cm^{-1} during the anodic process even for t=600 s. We only observed a shape changes of the peak at 1370 cm^{-1}, possibly due to the oxidative electrochemical decomposition of the CH_3CN solvent.

Table 3. Variation of the Raman spectra parameters of graphite during anodic intercalation in 1 M $NaClO_4/CH_3CN$

1 M $NACLO_4/CH_3CN$					
Time (s)	ω_{CH3} (cm^{-1})	Γ_{CH3} (cm^{-1})	ω_G (cm^{-1})	Γ_G (cm^{-1})	*n*
0 s	1372	11.8	1578	14.2	-
60 s	1371	9.7	1580	11.6	9.6
300 s	1371	10.0	1583	10.4	2.9
600 s	1369	20.6	1584	12.6	2.6

On the other hand, the growth of a significant P2 peak (Figure 8b) demonstrated a significant intercalation of solvated ClO_4^- anions, with no increase of defects (which would yield a P3 peak) and no mechanical exfoliation observed on microns scale. The intercalation stage index *n* (estimated from equation 1) reached $n \approx 3$ (600 s) showing a much more efficient intercalation as compared to sulfate ions in water (see in Table 3). Obviously, water-free electrolytes could achieve an efficient intercalation of organic molecule and inorganic anions without the damage of graphite lattice even under an anodic process. The efficient intercalation is not sufficient *per se* to achieve significant exfoliation

View Article Online
DOI: 10.1039/C9FD00123A

but should be followed by a chemical decomposition of the intercalants, with gas production. The ideal process would thus combine first an efficient intercalation of suitable ions (e.g. ClO_4^- in acetonitrile) followed by successive decomposition of such ions. This procedure has been already tested experimentally by us in a previous work[17], in which graphite was intercalated by perchlorate ions and acetonitrile molecules under a + 5 V potential for 30 minutes, and further expanded under microwave irradiation due to the degradation of the co-intercalated organic molecules. The in-situ measurements performed here gives thus an experimental support to our empirical procedure, and demonstrates the better potential of a two-stage exfoliation procedure to achieve high yield and low defectivity at the same time.

Conclusion

In summary, we compared the anodic graphite exfoliation process in dilute acid (0.5 M H_2SO_4) and neutral salt (0.5 M Li_2SO_4) electrolytes by *in-situ* optical and Raman spectroscopy analysis. In either acidic or neutral aqueous media, blistering and cracking was observed on the uppermost graphite layers. The relative anion intercalation, graphite oxidation and mechanical expansion steps were correlated to Raman I_D/I_G ratio and G band splitting variations. Our observation gives a deep understanding for the mechanism of EGO formation in aqueous electrolytes. We also demonstrated that the use of nonaqueous electrolyte (1 M $NaClO_4/CH_3CN$) is an alternative for efficient graphite intercalation without oxidation. The combination of efficient, non-destructive intercalation followed by chemical decomposition of the intercalants and gas production seems thus the best way to exfoliate graphite by an anodic intercalation process.

Conflicts of interest

The authors declare no conflict of interest.

Acknowledgements

The research leading to these results has received funding from the European Union's Horizon 2020 research and innovation programme under GrapheneCore2 785219 −

View Article Online
DOI: 10.1039/C9FD00123A

Graphene Flagship and from the Swedish Research Council under project (project Janus 2017-04456).

Reference:

1. M. S. Dresselhaus and G. Dresselhaus, *Advances in Physics*, 1981, **30**, 139-326.
2. J. B. Goodenough and Y. Kim, *Chemistry of Materials*, 2010, **22**, 587-603.
3. C. Sole, N. E. Drewett and L. J. Hardwick, *Faraday Discussions*, 2014, **172**, 223-237.
4. A. Ambrosi and M. Pumera, *Chemistry-a European Journal*, 2013, **19**, 4748-4753.
5. S. Yang, M. R. Lohe, K. Mullen and X. L. Feng, *Advanced Materials*, 2016, **28**, 6213-6221.
6. F. Beck, J. Jiang and H. Krohn, *Journal of Electroanalytical Chemistry*, 1995, **389**, 161-165.
7. J. Z. Wang, K. K. Manga, Q. L. Bao and K. P. Loh, *Journal of the American Chemical Society*, 2011, **133**, 8888-8891.
8. A. Ejigu, I. A. Kinloch and R. A. W. Dryfe, *Acs Applied Materials & Interfaces*, 2017, **9**, 710-721.
9. A. J. Cooper, N. R. Wilson, I. A. Kinloch and R. A. W. Dryfe, *Carbon*, 2014, **66**, 340-350.
10. H. P. Lei, J. G. Tu, Z. J. Yu and S. Q. Jiao, *Acs Applied Materials & Interfaces*, 2017, **9**, 36702-36707.
11. P. Yu, Z. M. Tian, S. E. Lowe, J. C. Song, Z. R. Ma, X. Wang, Z. J. Han, Q. L. Bao, G. P. Simon, D. Li and Y. L. Zhong, *Chemistry of Materials*, 2016, **28**, 8429-8438.
12. Z. Y. Xia, D. Wei, E. Anitowska, V. Bellani, L. Ortolani, V. Morandi, M. Gazzano, A. Zanelli, S. Borini and V. Palermo, *Carbon*, 2015, **84**, 254-262.
13. Z. Y. Xia, S. Pezzini, E. Treossi, G. Giambastiani, F. Corticelli, V. Morandi, A. Zanelli, V. Bellani and V. Palermo, *Advanced Functional Materials*, 2013, **23**, 4684-4693.
14. M. Thompson, http://www.talgaresources.com/IRM/PDF/1742/TalgaReducesGraphite ProcessingStepsForLiionBatteries, 2016.
15. C. Y. Su, A. Y. Lu, Y. P. Xu, F. R. Chen, A. N. Khlobystov and L. J. Li, *Acs Nano*, 2011, **5**, 2332-2339.
16. K. Parvez, R. J. Li, S. R. Puniredd, Y. Hernandez, F. Hinkel, S. H. Wang, X. L. Feng and K. Mullen, *Acs Nano*, 2013, **7**, 3598-3606.

View Article Online
DOI: 10.1039/C9FD00123A

17. Z. Y. Xia, G. Giambastiani, C. Christodoulou, M. V. Nardi, N. Koch, E. Treossi, V. Bellani, S. Pezzini, F. Corticelli, V. Morandi, A. Zanelli and V. Palermo, *Chempluschem*, 2014, **79**, 439-446.
18. S. Pei, Q. Wei, K. Huang, H. M. Cheng and W. Ren, *Nat Commun*, 2018, **9**, 145.
19. J. Y. Cao, P. He, M. A. Mohammed, X. Zhao, R. J. Young, B. Derby, I. A. Kinloch and R. A. W. Dryfe, *Journal of the American Chemical Society*, 2017, **139**, 17446-17456.
20. G. Bussetti, R. Yivlialin, D. Alliata, A. L. Bassi, C. Castiglioni, M. Tommasini, C. S. Casari, M. Passoni, P. Biagioni, F. Ciccacci and L. Duo, *Journal of Physical Chemistry C*, 2016, **120**, 6088-6093.
21. C. Casiraghi, S. Pisana, K. S. Novoselov, A. K. Geim and A. C. Ferrari, *Applied Physics Letters*, 2007, **91**, 233108.
22. J. B. Wu, M. L. Lin, X. Cong, H. N. Liu and P. H. Tan, *Chemical Society Reviews*, 2018, **47**, 1822-1873.
23. E. Treossi, M. Melucci, A. Liscio, M. Gazzano, P. Samori and V. Palermo, *Journal of the American Chemical Society*, 2009, **131**, 15576-15577.
24. A. A. Muhsan and K. Lafdi, *Sn Applied Sciences*, 2019, **1**, 276.
25. K. Wiesener, *Electrochimica Acta*, 1973, **18**, 185-189.
26. G. Carotenuto, A. Longo, L. Nicolais, S. De Nicola, E. Pugliese, M. Ciofini, M. Locatelli, A. Lapucci and R. Meucci, *Journal of Physical Chemistry C*, 2015, **119**, 15942-15947.
27. S. Solin and H. Zabel., Graphite Intercalation Compounds, *Springer-Verlag*: Berlin, 1990.
28. G. Maccaferri, C. Zanardi, Z. Y. Xia, A. Kovtun, A. Liscio, F. Terzi, V. Palermo and R. Seeber, *Carbon*, 2017, **120**, 165-175.
29. L. G. Cancado, K. Takai, T. Enoki, M. Endo, Y. A. Kim, H. Mizusaki, A. Jorio, L. N. Coelho, R. Magalhaes-Paniago and M. A. Pimenta, *Applied Physics Letters*, 2006, **88**, 163106.
30. M. S. Dresselhaus, A. Jorio, A. G. Souza and R. Saito, *Philosophical Transactions of the Royal Society a-Mathematical Physical and Engineering Sciences*, 2010, **368**, 5355-5377.
31. D. C. Alsmeyer and R. L. McCreery, *Analytical Chemistry*, 1992, **64**, 1528-1533.
32. A. Pandy, Z. W. Yang, M. Gummalla, V. V. Atrazhev, N. Y. Kuzminyh, V. I. Sultanov and S. Burlatsky, *Journal of the Electrochemical Society*, 2013, **160**, F972-F979.
33. R. M. Tamgadge and A. Shukla, *Electrochimica Acta*, 2019, **325**, 134933.
34. B. G. Oliver and G. J. Janz, *Journal of Physical Chemistry*, 1970, **74**, 3819-3822.

View Article Online
DOI: 10.1039/C9FD00123A